Materials Research Letters

ISSN: (Print) (Online) Journal homepage: https://www.tandfonline.com/loi/tmrl20

Environmental transmission electron microscopy study of hydrogen charging effect on a Cu-Zr metallic glass

Lin Tian , Yue-Qing Yang , Tobias Meyer , Dominik Tönnies , Vladimir Roddatis , Hendrik Voigt , Xin-Ai Zhao , Zhang-Jie Wang , De-Gang Xie , Michael Seibt , Cynthia A. Volkert & Zhi-Wei Shan

To cite this article: Lin Tian , Yue-Qing Yang , Tobias Meyer , Dominik Tönnies , Vladimir Roddatis , Hendrik Voigt , Xin-Ai Zhao , Zhang-Jie Wang , De-Gang Xie , Michael Seibt , Cynthia A. Volkert & Zhi-Wei Shan (2020) Environmental transmission electron microscopy study of hydrogen charging effect on a Cu-Zr metallic glass, Materials Research Letters, 8:12, 439-445, DOI: 10.1080/21663831.2020.1791273

To link to this article: https://doi.org/10.1080/21663831.2020.1791273

MATER. RES. LETT.
2020, VOL. 8, NO. 12, 439–445
https://doi.org/10.1080/21663831.2020.1791273

MATERIALS RESEARCH LETTERS
Taylor & Francis
Taylor & Francis Group

ORIGINAL REPORT

Environmental transmission electron microscopy study of hydrogen charging effect on a Cu-Zr metallic glass

Lin Tian [a,b], Yue-Qing Yang [a], Tobias Meyer [c], Dominik Tönnies[b], Vladimir Roddatis [b,d], Hendrik Voigt[c], Xin-Ai Zhao[a], Zhang-Jie Wang[a], De-Gang Xie [a], Michael Seibt [c], Cynthia A. Volkert[b] and Zhi-Wei Shan [a]

[a]Center for Advancing Materials Performance from the Nanoscale (CAMP-NANO) and Hysitron Applied Research Center in China (HARCC), State Key Laboratory for Mechanical Behavior of Materials, Xi'an Jiaotong University, Xi'an, People's Republic of China; [b]Institute of Materials Physics, University of Göttingen, Göttingen, Germany; [c]4th Physical Institute – Solids and Nanostructures, University of Göttingen, Göttingen, Germany; [d]German Research Centre for Geosciences (GFZ), Helmholtz-Centre Potsdam, Potsdam, Germany

ABSTRACT

Hydrogen induced plasticity has been found in metallic glasses; however, the underlying mechanism remains unclear. Herein, we studied a Cu-Zr metallic glass charged in a hydrogen atmosphere inside an environmental transmission electron microscope. Compression tests of hydrogen charged nanopillars show more controllable deformation compared to uncharged ones. A variable resolution fluctuation electron microscopy study of the hydrogen charged samples reveals an increase in the correlation length of the medium-range order. Our results provide experimental evidence for hydrogen-induced heterogeneity and support the idea that increasing the degree of heterogeneity leads to multiple local shear events and suppresses catastrophic shear banding.

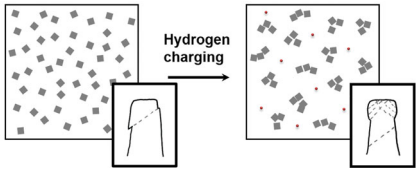

IMPACT STATEMENT

Direct evidence of an increase in the spatial correlation length of the medium-range order is found during hydrogen charging of a Cu-Zr metallic glass and leads to enhanced plastic deformation.

ARTICLE HISTORY
Received 21 April 2020

KEYWORDS
Correlation length; hydrogen; metallic glass; plasticity; variable resolution fluctuation electron microscopy

1. Introduction

The structure and properties of metallic glasses (MG) have been found to be heterogeneous at various length scales [1–4]. Heterogeneities in elastic modulus [5], medium-range order [6], density [7] and relaxation behavior [8,9], all have great impact on the mechanical properties of metallic glasses. On the one hand, heterogeneities in MGs evolve with deformation. Ross et al. [10] compared the nanoscale elastic heterogeneities between an as-cast and a fatigued $Zr_{50}Cu_{40}Al_{10}$ MG and observed an increase in the contact stiffness distribution induced by the cyclic mechanical loading. On the other hand, changing the degree of heterogeneity of MGs in the initial state gives rise to distinct deformation behavior during mechanical testing. Zhu et al. [11] reported that hyper quenched $Zr_{53}Cu_{36}Al_{11}$ MG has higher degree of heterogeneity, a larger excess enthalpy and is less brittle than its highly relaxed counterpart. By simulation studies, Wang et al. [12] showed the non-linear relationship between spatial correlation lengths of structural heterogeneities and plasticity of MGs. Thus, describing structural heterogeneities and correlating them with deformation behav-

CONTACT Lin Tian ltian@phys.uni-goettingen.de Center for Advancing Materials Performance from the Nanoscale (CAMP-NANO) and Hysitron Applied Research Center in China (HARCC), State Key Laboratory for Mechanical Behavior of Materials, Xi'an Jiaotong University, Xi'an 710049, People's Republic of China; Institute of Materials Physics, University of Göttingen, Göttingen 37077, Germany; Cynthia A. Volkert volkert@ump.gwdg.de Institute of Materials Physics, University of Göttingen, Göttingen 37077, Germany; Zhi-Wei Shan zwshan@mail.xjtu.edu.cn Center for Advancing Materials Performance from the Nanoscale (CAMP-NANO) and Hysitron Applied Research Center in China (HARCC), State Key Laboratory for Mechanical Behavior of Materials, Xi'an Jiaotong University, Xi'an 710049, People's Republic of China

Supplemental data for this article can be accessed here. https://doi.org/10.1080/21663831.2020.1791273

ior is important for understanding the amorphous structure and its deformation mechanism.

Hydrogen charging is expected to change the heterogeneities in metallic glasses [13,14]. However, the mechanism of how hydrogen changes the amorphous structure remains unclear and direct evidence of structural changes, especially the changes in heterogeneities which lead to different mechanical behavior, is still missing. In this work, the effect of hydrogen charging on the structure and mechanical properties of a $Cu_{49}Zr_{51}$ MG are studied using an environmental transmission electron microscope (ETEM) with the aim of pinpointing the key structural parameters that govern the mechanical properties and deformation mechanisms of MGs. Taking advantage of the ETEM, the structure of the hydrogen charged samples can be characterized directly using variable resolution fluctuation electron microscopy (VR-FEM) to measure the correlation length of the medium-range order.

2. Methods

2.1. Sample preparation

A Cu_{49} Zr_{51} MG ribbon with the thickness of $\sim 40\,\mu$m was prepared using melt spinning. Cylindrical nanopillars with radius ~ 200 nm were fabricated on the edge of the ribbon via focused ion beam (FIB, FEI Helios NanoLab 600) milling with 30 keV gallium ion currents from 2.8 nA to 28 pA. The gradually reduced current was used to minimize the surface damage and pillar taper angles.

2.2. Hydrogen charging and in situ mechanical test in TEM

The *in situ* TEM nanocompression tests were performed with a Hysitron PI95 H1H PicoIndenter. Mechanical test in a vacuum and in ~ 2 Pa hydrogen gas were observed in real-time in an ETEM (Hitachi H-9500) operating at 300 kV and 4uA emission current. Before the tests in hydrogen atmosphere, the pillars were charged under electron beam exposure with a current density of 2.55×10^{-11}C/cm^2 in hydrogen gas for about 2 h.

2.3. Mechanical controllability index (MCI) calculation

To quantitatively estimate the stability of deformation of nanopillars under compression, the mechanical controllability index (MCI) was calculated [15]. A 'controllable plastic strain' $\varepsilon_P^{\text{control}}$ is defined as

$$\varepsilon_P^{\text{control}} = \int d\varepsilon_P \Theta(\rho(\varepsilon_P) - \text{CSR}^{-1}), \qquad (1)$$

where $\rho(\varepsilon_P)$ is the 'density-of-states' of plastic-strain [15], $\Theta()$ is the Heaviside step function ($\Theta(x > 0) = 1$ and $\Theta(x \leq 0) = 0$), and CSR is a 'critical strain rate' parameter which is set to 0.1/second according to the data collection rate. The $\varepsilon_P^{\text{control}}$ is the plastic strain of the sample minus the strain bursts. The MCI index represents the portion of the total plastic strain which is controllable and is calculated by,

$$\text{MCI} = -\ln(1 - \varepsilon_P^{\text{control}}/\varepsilon_P^{\text{total}}). \qquad (2)$$

A cutoff at a total strain of 15% is applied to exclude the large strain bursts in all the samples at large strains. According to Equation (2), a low MCI is expected when obvious strain bursts occurs in the stress–strain curve, with MCI $= 0$ meaning completely uncontrollable plastic deformation and MCI $= \infty$ indicating totally controllable plastic deformation. In metallic glasses, shear band formation results in intermittent plasticity thus a low MCI. An increase MCI indicate a more controllable deformation and improved plasticity. Detailed definitions and descriptions of the MCI have been reported in [15].

2.4. Variable resolution fluctuation electron microscopy

Fluctuation electron microscopy (FEM) has been successfully used to characterize structural heterogeneities in amorphous materials [16,17]. Variable resolution fluctuation electron microscopy (VR-FEM) [18,19], collects FEM data using electron probes with different sizes and uses these to determine the correlation length of the structural heterogeneities. In this study, VR-FEM is carried out on a lamella prepared by FIB milling in an ETEM (Thermo Fisher Scientific FEI E-TEM) on the same sample with and without hydrogen charging. The hydrogen charging procedure is the same as that of the pillars except that the hydrogen pressure is ~ 200 Pa, 100 times of that of the pillars to make sure hydrogen charging results in detectable structural changes. The nanobeam diffraction mapping is operated in the 'microprobe' mode with the C2 condenser lens aperture of 10 µm. By tuning the convergence angle between 0.7 and 0.25 mrad, different probe sizes $R = 2.0$, 2.5, 3.5, 4.4, and 6.2 nm can be achieved. After changing the convergence angle, the beam current is finely adjusted to keep a constant value (~ 15 pA) and the beam alignment is optimized in order to keep the coherence as consistent as possible for the different probe sizes. The exposure time is set to 2 s, long enough to ensure a good signal-to-noise ratio but not too long to lead to obvious sample drift. The FEM data sets are taken from the same region of the sample

to get direct comparison of the structure with and without hydrogen. To control possible contamination in the region of interest, which is scanned multiple times, the sample is cleaned using a plasma cleaner for 30 s right before being inserted into the TEM chamber. The characteristic correlation length Λ is calculated using pair persistence analysis [16,20].

3. Results

3.1. In situ compression of pillars in a vacuum and hydrogen gas

Engineering stress–strain curves of three of the eight pillars compressed in a vacuum and three out of nine pillars compressed in hydrogen gas with low, medium and high MCIs are shown in Figure 1(a,b) respectively. From the stress–strain curves of P1–P3 in Figure 1(a) which are tested in a vacuum, one can observe multiple strain bursts and stress drops. In contrast, the curves of some pillars tested in hydrogen gas, for instance P5 and P6, are more continuous.

Figure 1(c–f) are images of P1 which is a typical low MCI pillar at different strains corresponding to the points marked in its stress–strain curve. Shear steps of shear bands are captured at strain ~7% (Figure 1d) and ~12% (Figure 1e). When strain reaches ~20% a large strain burst occurs, see the Supplementary Movie 1. Movie frames from the compression process of P6 which was charged with hydrogen and has the highest MCI in all pillars are presented in Figure 1(g–j). Different from the deformation in a vacuum, there are no significant strain bursts until the engineering strain reaches 22%, see Figure 1(j). As shown in Figure 1(h,i), the typical 'mushroom' morphology develops in the top part of pillar P6, which indicates that relatively uniform deformation with no visible shear bands is occurring in the top region of the pillar.

The average MCI of hydrogen charged pillars is 2.58 ± 1.41, about 2.2 time of that of pillars compressed in a vacuum which is 1.16 ± 0.3. This increase in MCI implies improved plasticity induced by hydrogen charging. It should be noted that some hydrogen charge pillars deform via shear banding. For instance, the stress–strain curve of P4 displays multiple strain bursts. This instability in the deformation is well characterized by its low MCI. The large scattering in MCI for hydrogen charged pillars presumably reflects the increase in degree of heterogeneity caused by hydrogen incorporation. The yield strength (defined as the onset of major shear band formation or strength at 2% offset strain) vs the MCIs of all tested pillars are summarized in Figure 2. Their

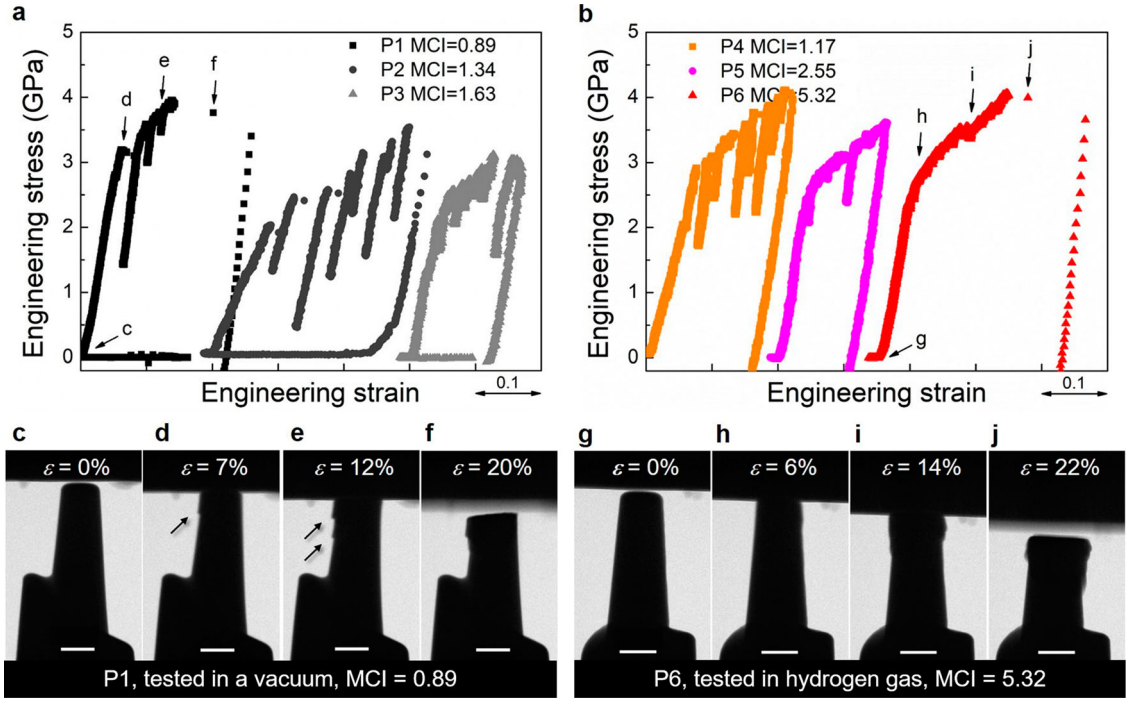

Figure 1. The *in situ* compression of Cu-Zr nanopillars in a vacuum and hydrogen gas. Typical engineering stress versus strain curves of nanocompression tests in a vacuum (a) and hydrogen gas (b). (c)–(f) correspond to the marked points in a vacuum tested P1 in (a) with a low MCI. (g)–(j) denote the marked points in compression of hydrogenated P3 in (b) which has the largest MCI. The scale bar in each figure represents 200 nm. See also the recorded movie in Supplementary Materials.

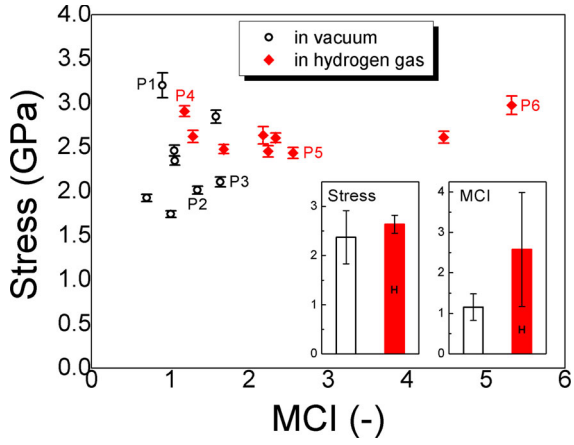

Figure 2. The comparison of yield strength and MCI between pillars tested in a vacuum and hydrogen gas. The data points corresponding to the stress-strain curves in Figure 1 are marked by the pillar numbers.

strength is unchanged within the noise, see the insets in Figure 2.

3.2. VR-FEM during hydrogen charging

To study the amorphous structure with and without hydrogen, a Cu-Zr lamella prepared using FIB is measured by nanobeam diffraction before and during hydrogen charging. FEM datasets are first collected on the uncharged sample with five different sequential electron probe sizes, $R = 2.0$, 2.5, 3.5, 4.4, and 6.2 nm. The FEM variance curves, shown in Figure 3(a), feature two main peaks, with the first one located at a scattering vector of $k = 4.2\,\mathrm{nm}^{-1}$. Before hydrogen charging, the probe size is set back to 2.0 nm and tuned to get the same beam conditions. Then the hydrogen charging is started keeping the e-beam unchanged. After the sample is immersed in hydrogen gas for 2 h, FEM datasets are collected again with the five different probes. The variance curves for the 2.0 and 6.2 nm probes collected before and during hydrogen charging are plotted in Figure 3(a). The average of 3–5 curves are plotted as a solid line with the colored bands indicate the standard deviation. The variance V of the 2.0 nm probe data is higher than the 6.2 nm probe data, which is typical for metallic glasses [19]. After the sample has been charged with hydrogen, the variance curves of the smallest probe of 2.0 nm decrease while those of the largest probe of 6.2 nm increase. As indicated by the black and red arrows in Figure 3(a) and summarized in Figure 3(b), the difference in variance (at $k = 4.2\,\mathrm{nm}^{-1}$) between the smallest and largest probes decreases after the sample is charged with hydrogen. FEM datasets are collected again 2 h after the hydrogen was pumped out and the variances are shown as the closed squares in Figure 3(b). The recovery of the variance values suggests that hydrogen has left the sample.

The correlation length Λ is determined from a linear fit to a plot of Q^2/V against Q^2 in Figure 3(c). Q is the radius of a virtual objective aperture (in reciprocal space units) and is related to the probe size R by $Q = 0.61/R$. According to the pair-persistence analysis [18], $\Lambda = \frac{1}{2\pi}\sqrt{\frac{b}{a}}$ where a is the intercept and b is the slope. The correlation length Λ of the sample is 1.25 ± 0.44 nm before hydrogen charging and increases to 1.58 ± 0.60 nm with hydrogen. See the supporting information for details of the error analysis. There is no clear evidence for structural expansion in the variance curve due to hydrogen charging, presumably because of the lower k resolution of electron diffraction relative to x-ray diffraction. No evidence for hydrides was found in the hydrogen charged sample.

4. Discussion

We employed VR-FEM to study the correlation length Λ of the medium-range order with the scattering vector $k = 4.2\,\mathrm{nm}^{-1}$ at the first main peak in both variance and scattering intensity. The correlation of the medium-range order is described by the correlation coefficient $\rho(r) = exp\left(-\frac{r^2}{2\Lambda^2}\right)$ [18]. As illustrated by the two curves in Figure 4(a), the correlation coefficient in materials with a larger Λ (curve 2) drops more slowly than in materials with a smaller Λ (curve 1). To visualize the change in Λ, the specific medium-range order which contributes to the scattering events at $k = 4.2\,\mathrm{nm}^{-1}$ is depicted as squares in Figure 4(b,c). An increase in Λ then corresponds to a change in spatial distribution (Figure 4b–c), without a change in average number density. The constant number density is supported by the almost identical intensity profiles of diffraction patterns. In these simplified 2D cases (representative cross-sections of a 3D volume), Λ can be seen as a measure of the size of the regions containing the specific medium-range order [21]. The increase in Λ corresponds to a tendency of agglomeration as illustrated by Figure 4(c) compared to Figure 4(b). These sketches represent a possible scenario of the structural evolution during hydrogen charging which can be induced by the preferential occupation of hydrogen in the amorphous structure given the affinity of hydrogen to Zr rich sites [22]. As a result of the local rearrangement induced by hydrogen incorporation, e.g. reducing shared atoms between specific clusters [23], the Λ increases and the degree of heterogeneity of the entire amorphous structure also increases. The measurement of variance

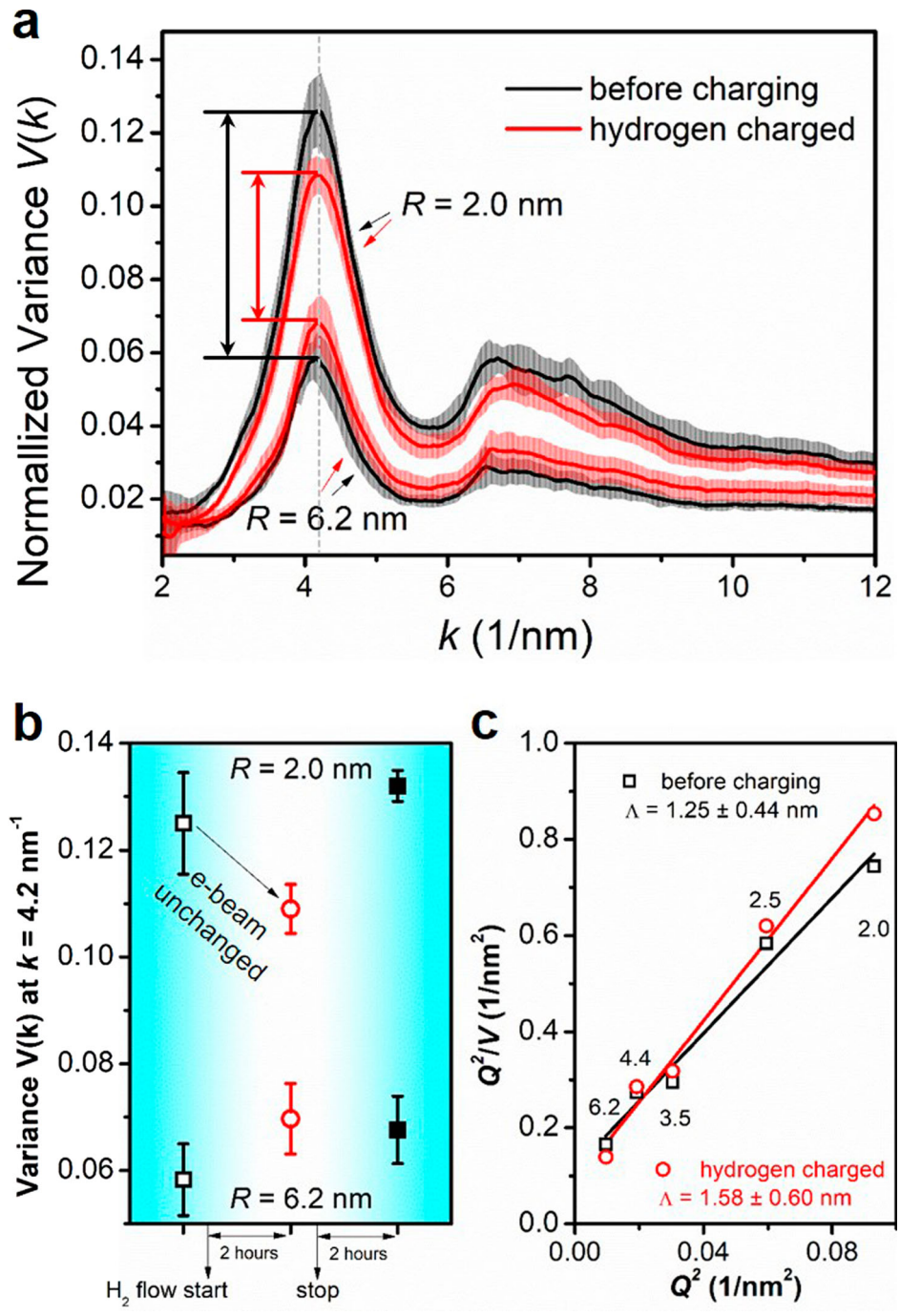

Figure 3. Variance resolution fluctuation electron microscopy study of the amorphous structure. (a) Variance curves of the sample before and during hydrogen charging using electron beam probe sizes of 2.0 and 6.2 nm. (b) The evolution of the variance at $k = 4.2\,\mathrm{nm}^{-1}$ before charging, after 2 h' hydrogen exposure and 2 h after hydrogen is pumped out. (c) Pair-persistence analysis and calculation of the correlation length of the sample before and during hydrogen charging.

of the sample after hydrogen gas was pumped out suggests that this increase in Λ during hydrogen charging is reversible and hydrogen tends to leave the sample in a vacuum.

It has been predicted by simulations [12] that enhanced degree of heterogeneity increases the plasticity of metallic glasses. The hydrogen charged structure offers more sites for the activation of local shear events, which leads to distribute plastic flow [12]. Consequently, catastrophic shear bands are postponed as clearly evidenced by the morphology of pillars compressed in hydrogen gas (see a schematic in Figure 4d) compared to that of pillars

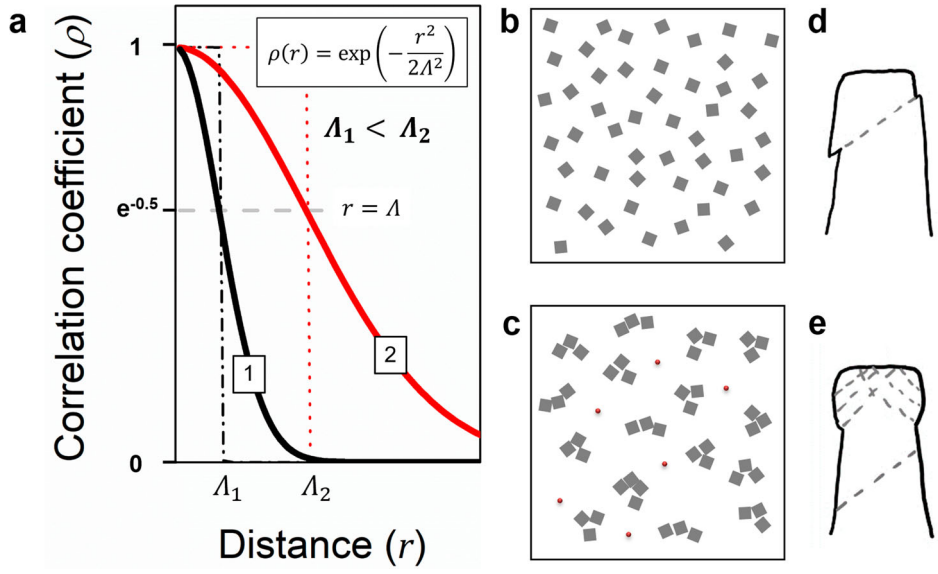

Figure 4. A schematic of structure change induced by hydrogen charging. (a) The correlation coefficient as a function of distance. The correlation length Λ is defined when $e^{-0.5} = 0.607$ and $r = \Lambda$. (b–c) The distribution of medium-range order in 2D view before and after hydrogen charging. (d–e) Deformation morphology with and without hydrogen.

tested in a vacuum (Figure 4e). Our ETEM experiments confirms co-occurrence of increased degree of heterogeneity and improved plasticity, thus, support the theoretical prediction. While the plasticity is improved, the strength remains unchanged by hydrogen charging. This observation agrees with our recent work [24] and also the work of other groups [14,25] on bulk MG samples. Indeed, the strength of the hydrogen charged pillars as shown in Figure 2 has narrower distribution than that of pillars without hydrogen while the distribution of MCIs increases. The pillars without hydrogen, on the contrary, sometimes suffer from early shear bands occurring at low stresses. We infer that the hydrogen addition in metallic glasses can heal some defects in the amorphous structure by filling small voids and free volumes, while at the same time increasing the variation in local structure at the nm scale. Further studies are needed to understand hydrogen charged metallic glasses from atomic scale.

5. Conclusions

In this work, we studied the effect of hydrogen charging on the structure and mechanical properties of a Cu-Zr metallic glass. Compression tests of hydrogen charged MG pillars in an ETEM reveal more controllable deformation without sacrificing strength. VR-FEM analysis indicates an increase in the correlation length of medium-range order in the hydrogen charged sample. This work provides first direct experimental support for the idea that the spatial distribution of medium-range order in a MG control the extent of plasticity. We show also that hydrogen charging can be used to tune the heterogeneities and the plasticity.

Acknowledgements

L.T. acknowledges Natural Science Foundation of China (Grant 51501144), China Postdoctoral Science Foundation (2015M580842), and the Alexander von Humboldt foundation for financial support. C.A.V. and D.T. acknowledge financial support by the Deutsche Forschungsgemeinschaft (DFG, German Research Foundation) - VO 928/9-1. Z.W.S. and D.G.X. acknowledge support by the National Key Research and Development Program of China (No. 2017YFB0702001) and Natural Science Foundation of China (51971169, 51701151, 51231005 and 51621063). T.M. and M.S. knowledge funding by the Deutsche Forschungsgemeinschaft (DFG, German Research Foundation) - 217133147/SFB 1073, projects B02, Z02. L.T. thanks Matthias Hahn for assistance in in-situ hydrogen charging experiments.

Disclosure statement

No potential conflict of interest was reported by the author(s).

Funding

L.T. acknowledges National Natural Science Foundation of China [grant number 51501144], China Postdoctoral Science Foundation [grant number 2015M580842], and the Alexander von Humboldt foundation for financial support. C.A.V. and D.T. acknowledge financial support by the Deutsche Forschungsgemeinschaft (DFG) in an individual [grant number VO 928/9-1]. Z.W.S. and D.G.X. acknowledge support by the National Key Research and Development Program of China [grant number 2017YFB0702001] and National Natural Science Foundation of China [grant numbers 51971169,

51701151, 51231005 and 51621063]. T.M. and M.S. knowledge funding by the Deutsche Forschungsgemeinschaft (DFG, German Research Foundation) - 217133147/SFB 1073, projects B02, Z02.

ORCID

Lin Tian http://orcid.org/0000-0003-3841-3946
Yue-Qing Yang http://orcid.org/0000-0001-6772-5776
Tobias Meyer http://orcid.org/0000-0003-3191-0376
Vladimir Roddatis http://orcid.org/0000-0002-9584-0808
De-Gang Xie http://orcid.org/0000-0001-7658-2738
Michael Seibt http://orcid.org/0000-0002-9908-400X
Zhi-Wei Shan http://orcid.org/0000-0002-4533-0869

References

[1] Li M, Wang CZ, Hao SG, et al. Structural heterogeneity and medium-range order in Zr_xCu_{100-x} metallic glasses. Phys Rev B. 2009;80:184201.
[2] Liu C, Maaß R. Elastic fluctuations and structural heterogeneities in metallic glasses. Adv Funct Mater. 2018;28:1800388.
[3] Tian L, Volkert CA. Measuring structural heterogeneities in metallic glasses using transmission electron microscopy. Metals. 2018;8:1085.
[4] Qiao JC, Wang Q, Pelletier JM, et al. Structural heterogeneities and mechanical behavior of amorphous alloys. Prog Mater Sci. 2019;104:250–329.
[5] Wagner H, Bedorf D, Kuchemann S, et al. Local elastic properties of a metallic glass. Nat Mater. 2011;10:439–442.
[6] Hart MJ, Bassiri R, Borisenko KB, et al. Medium range structural order in amorphous tantala spatially resolved with changes to atomic structure by thermal annealing. J Non-Cryst Solids. 2016;438:10–17.
[7] Zhu F, Hirata A, Liu P, et al. Correlation between local structure order and spatial heterogeneity in a metallic glass. Phys Rev Lett. 2017;119:215501.
[8] Zhang P, Maldonis JJ, Liu Z, et al. Spatially heterogeneous dynamics in a metallic glass forming liquid imaged by electron correlation microscopy. Nat Commun. 2018;9:1129.
[9] Wang Z, Wang WH. Flow units as dynamic defects in metallic glassy materials. Natl Sci Rev. 2018;6:2095–5138.
[10] Ross P, Küchemann S, Derlet PM, et al. Linking macroscopic rejuvenation to nano-elastic fluctuations in a metallic glass. Acta Mater. 2017;138:111–118.
[11] Zhu F, Song S, Reddy KM, et al. Spatial heterogeneity as the structure feature for structure–property relationship of metallic glasses. Nat Commun. 2018;9:3965.
[12] Wang N, Ding J, Yan F, et al. Spatial correlation of elastic heterogeneity tunes the deformation behavior of metallic glasses. NPJ Comput Mater. 2018;4:1–10.
[13] Granata D, Fischer E, Löffler JF. Hydrogen microalloying as a viable strategy for enhancing the glass-forming ability of Zr-based bulk metallic glasses. Scripta Mater. 2015;103:53–56.
[14] Zhao Y, Choi IC, Seok MY, et al. Hydrogen-induced hardening and softening of Ni–Nb–Zr amorphous alloys: Dependence on the Zr content. Scripta Mater. 2014;93:56–59.
[15] Wang ZJ, Shan ZW, Ju L, et al. An index for deformation controllability of small-volume materials. Sci China Technol Sci. 2014;57:663–670.
[16] Treacy M, Gibson J. Variable coherence microscopy: a rich source of structural information from disordered materials. Acta Crystallogr Sect A. 1996;52:212–220.
[17] Voyles PM, Gibson JM, Treacy MMJ. Fluctuation microscopy: a probe of atomic correlations in disordered materials. J Electron Microsc. 2000;49:259–266.
[18] Gibson JM, Treacy MMJ, Voyles PM. Atom pair persistence in disordered materials from fluctuation microscopy. Ultramicroscopy. 2000;83:169–178.
[19] Hwang J, Voyles PM. Variable resolution fluctuation electron microscopy on Cu-Zr metallic glass using a wide range of coherent STEM probe size. Microsc Microanal. 2011;17:67–74.
[20] Bogle SN, Nittala LN, Twesten RD, et al. Size analysis of nanoscale order in amorphous materials by variable-resolution fluctuation electron microscopy. Ultramicroscopy. 2010;110:1273–1278.
[21] Murphy JN, Harris KD, Buriak JM. Automated defect and correlation length analysis of block copolymer thin film nanopatterns. PLoS One. 2015;10:1932–6203.
[22] Samwer K, Johnson W. Structure of glassy early-transition-metal-late-transition-metal hydrides. Phys Rev B. 1983;28:2907.
[23] Ding J, Ma E, Asta M, et al. Second-nearest-neighbor correlations from connection of atomic packing motifs in metallic glasses and liquids. Sci Rep. 2015;5:17429.
[24] Tian L, Tönnies D, Hirsbrunner M, et al. Effect of hydrogen charging on pop-in behavior of a Zr-based metallic glass. Metals. 2019;10:22.
[25] Luo LS, Wang BB, Dong FY, et al. Structural origins for the generation of strength, ductility and toughness in bulk-metallic glasses using hydrogen microalloying. Acta Mater. 2019;171:216–230.